

# Estimates of the Mutual Influence of Variations in the Sea Surface Temperature in Tropical Latitudes of the Pacific, Atlantic, and Indian Oceans from Long-Period Data Series

I. I. Mokhov<sup>a, b, \*</sup> and D. A. Smirnov<sup>c, d, \*\*</sup>

<sup>a</sup> *Obukhov Institute of Atmospheric Physics, Russian Academy of Sciences, Moscow, 119017 Russia*

<sup>b</sup> *Moscow State University, Moscow, 119991 Russia*

<sup>c</sup> *Saratov Branch of Kotel'nikov Institute of Radioengineering and Electronics, Russian Academy of Sciences, Saratov, 410019 Russia*

<sup>d</sup> *Institute of Applied Physics, Russian Academy of Sciences, Nizhny Novgorod, 603950 Russia*

\**e-mail: mokhov@ifaran.ru*

\*\**e-mail: smirnovda@yandex.ru*

Received October 5, 2016; in final form, December 9, 2016

**Abstract**—Based on the concept of the Wiener–Granger causality, a seasonal trivariate analysis of directional couplings between sea surface temperature variations in tropical latitudes of the Pacific, Atlantic, and Indian Oceans has been performed. These variations are related to significant modes of regional and global climatic variability. We have analyzed time series of monthly indices of Pacific Ocean processes of the El Niño/Southern Oscillation (ENSO), equatorial Atlantic mode (EAM), and Indian Ocean Dipole (IOD)—along with its western and eastern poles for the period of 1870–2015. A scheme of interactions between the processes under study where coupling strength estimates are presented, along with estimates of the season of its maximal value and the coupling coefficient sign, has been developed. We have found the seasonal influences of ENSO on the western and eastern poles of IOD, the eastern pole of IOD on ENSO, EAM on ENSO, and IOD on EAM to be the most significant couplings.

**Keywords:** El Niño/Southern Oscillation, equatorial Atlantic mode, Indian Ocean Dipole, time series analysis, Wiener–Granger causality, seasonal analysis of directional couplings

DOI: 10.1134/S0001433817060081

## 1. INTRODUCTION

Climatic variations in tropical latitudes due to anomalies of the sea surface temperature (SSTs) have a significant effect on the climatic regime of extratropical latitudes and terrestrial climatic system on the whole [1]. At the same time, they strongly affect the economy of regions inhabited by the majority of the Earth's population [2].

In tropical regions of the Pacific Ocean (PO), the key mode of the interannual OST variability is the El Niño/Southern Oscillation (ENSO) quasi-cyclic process manifesting itself, in particular, in the increase in the OST in the eastern and central regions with a periodicity in the range of 2–8 years. It is associated with strongest interannual variations in the global surface temperature [1]. The risk of anomalies in the temperature, hydrological, and circulation regimes in the atmosphere depends on the ENSO not only in tropical latitudes (see, e.g. [3–8]).

An analog of the ENSO in tropical latitudes of the Atlantic Ocean (AO) is the equatorial Atlantic mode

(EAM) manifesting itself in OST variations in the eastern part of the equatorial Atlantic [9, 10]. However, contrasts between the eastern and western regions in the equatorial Atlantic are less than in the Pacific Ocean, and typical temporal scales of 2–4 years are also less than for the ENSO. The difference in EAM and ENSO characteristics is significantly related to the lesser extension of the Atlantic basin in equatorial latitudes [10].

In tropical latitudes of the Indian Ocean (IO), a significant mode characterized by the difference of the OST in the western and eastern regions of the basin is the so-called Indian Ocean Dipole (IOD) with its western (IWP) and eastern (IEP) poles [11]. This mode is associated with strong regional variations in precipitations in tropical latitudes. Effects of climatic processes in tropical latitudes of the Atlantic and Indian Oceans manifest themselves also in extratropical latitudes, although less significantly than ENSO effects [2].

There are many investigations devoted to climatic processes occurring in tropical latitudes and having an effect on the global climate [1]. Of particular impor-

tance are investigations into the role of different factors in the SST dynamics of tropical oceans and relations between them [2, 12–24].

The investigations resulted in obtaining rather contradictory facts about the character of relations, e.g., about the directionality of the coupling between the ENSO and EAM. One of the reasons is probably the fact that cross-correlation functions and linear regressions of the analyzed characteristics of processes on simultaneous or preceding values of characteristics of other processes were the main quantitative tools for characterizing the couplings [12–14, 19, 23]. These approaches are good for revealing statistical dependences between processes and are often sufficient in estimating unidirectional couplings. However, their possibilities are severely limited when studying mutual impacts (bidirectional couplings) and do not allow one to definitely answer the question about cause-and-effect relations and strength of coupling between processes (systems) [27–31].

In view of the abovementioned problems, in the analysis of cause-and-effect relations it is suitable to pass from the usual cross correlation between the current value of one process and the future value of the second process to their conditional (partial) cross correlation [27–31]. One approach of this kind is the bivariate Wiener–Granger causality analysis, which is based on comparing prediction errors of empirical autoregressive models with allowance for data about one process and without regard for them when forecasting the second process [32, 33].

It is suitable to further develop an analysis of directional couplings of climatic processes in tropical latitudes of three oceans. In particular, the abovementioned investigations did not take into account the possible seasonal dependence of coupling forces and oscillator properties. In this work, the relationship of the aforesaid processes is systematically investigated based on the Wiener–Granger causality analysis with the use of trivariate autoregressive models with allowance for the possible seasonal dependence of coupling characteristics.

## 2. DATA USED AND THEIR CORRELATION CHARACTERISTICS

Climatic process in tropical Pacific, Atlantic, and Indian oceans were characterized by the ENSO, EAM, and IWP–IEP–IOD indices. The analysis involved monthly average HadISST data (<http://www.metoffice.gov.uk/>) for the SST for the period of 1870–2015.

The Niño 3.4 index characterizing OST anomalies in the equatorial region ( $5^{\circ}$  N– $5^{\circ}$  S,  $170^{\circ}$ – $120^{\circ}$  W) was used as an indicator of the ENSO process. The analysis was also carried out for the Niño 3 index ( $5^{\circ}$  N– $5^{\circ}$  S,  $90^{\circ}$ – $150^{\circ}$  W) with very close results.

For the Atlantic Ocean, the EAM index was used (SST in the region of  $3^{\circ}$  N– $3^{\circ}$  S,  $0^{\circ}$ – $20^{\circ}$  W in the Atlantic Ocean) by analogy with [10]. The IOD index was characterized by the difference of SST between the IWP (SST in the region of  $10^{\circ}$  N– $10^{\circ}$  S,  $50^{\circ}$ – $70^{\circ}$  E) and IEP ( $0^{\circ}$ – $10^{\circ}$  S,  $90^{\circ}$ – $110^{\circ}$  E) by analogy with [11]. Together with the IOD index, the indices for its two poles (IWP and IEP) were analyzed.

When analyzing the series of monthly average data for the SST from January 1870 to November 2015 (1751 months), the annual cycle was removed by subtracting average values for each month. The remaining long-period variations on decade scales were also excluded; they were approximated, in particular, by quadratic polynomials for the analyzed period. Below, the following notation is used for the corresponding variables:  $x_p$  is the ENSO index;  $x_A$  is the EAM index; and  $x_j$  is the IWP, IEP, or IOD index.

Features of the analyzed data are characterized in Fig. 1: average values of initial SSTs (Fig. 1a) and seasonal root-mean-square values of the indices  $x_p$ ,  $x_A$ , and  $x_j$  (Fig. 1b), as well as autocorrelation functions (ACFs) of these indices (Fig. 1c). The characteristic time of the ACF drop (to  $1/e$ ) for ENSO is 7 months, for EAM it is 4 months, for IWP it is 5 months, for IEP it is 4 months, and for IOD it is 3 months.

An analysis of cross correlation functions (CCFs) allows one to reveal the presence of couplings (Fig. 2), but not the action in a specific direction. In particular, in the appearance of the CCF for ENSO and IEP, one can suppose the unidirectional influence of ENSO on IEP (Fig. 2b) but the results of the analysis of directional couplings in this work testify also about the strong impact of IEP on ENSO; at the same time, the impacts of ENSO and IEP on each other are of different signs.

## 3. METHOD OF ANALYZING DIRECTIONAL COUPLINGS

The applied method of coupling estimation [32, 33] is based on an analysis of the Granger causality also called the Wiener–Granger causality [20, 27–30]. In the case of analyzing two processes  $x_j$  and  $x_k$ , the impact of the process  $x_j$  on the process  $x_k$  is characterized as the degree of dependence of the current value  $x_k$  on preceding values  $x_j$  at fixed preceding values  $x_k$ . A quantitative measure of the directional coupling is the difference between variances of prediction errors of two empirical autoregressive (AR) models—with allowance for  $x_j$  and without regard to them. If the third process  $x_i$  is taken into account, both the prediction errors are calculated for models with allowance for  $x_i$ . This brings the obtained characteristic closer to the estimate of the direct effect of  $x_j$  on  $x_k$ , i.e., the effect not via the chain  $x_j \rightarrow x_i \rightarrow x_k$ . Like any empir-

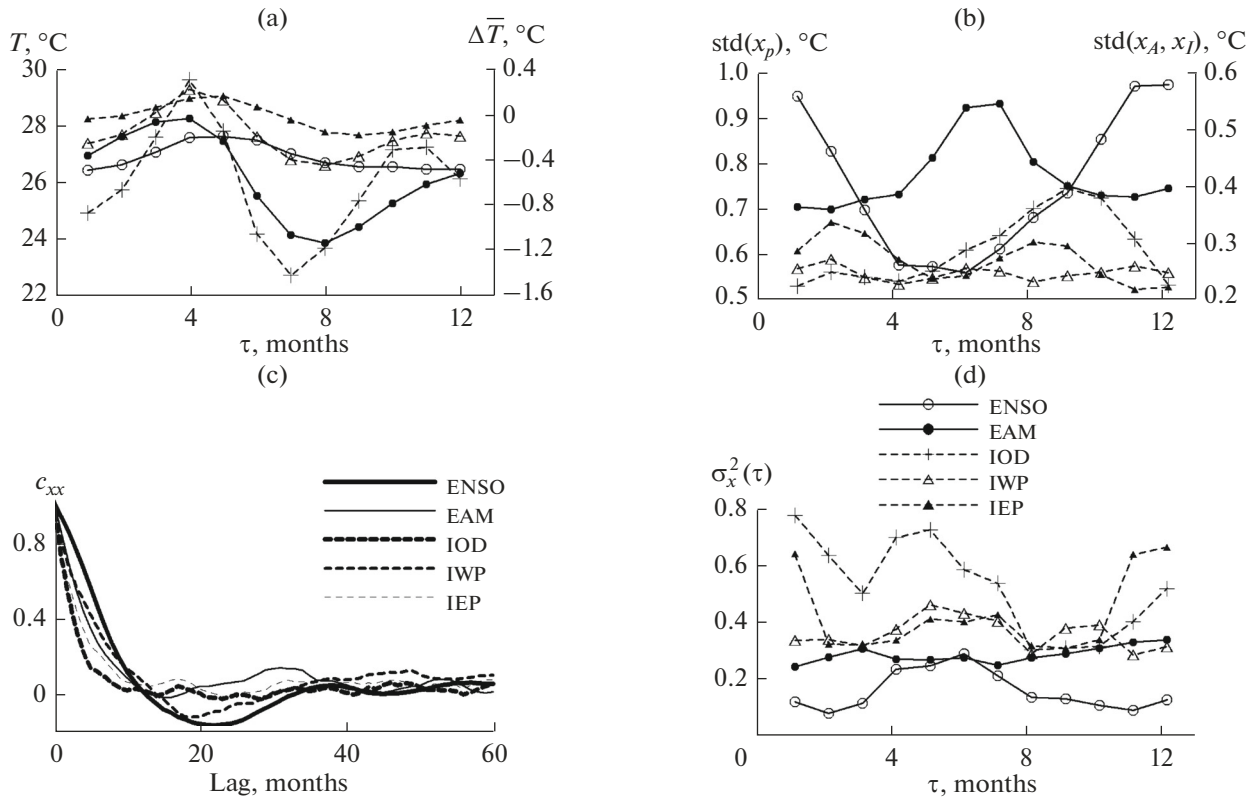


**Fig. 1.** Characteristics of the series under study for the ENSO, EAM, IOD, IWP, and IEP indices: (a) average many-year annual behavior of the SST and (b) corresponding root-mean-square deviations, (c) autocorrelation index functions of the gap, and (d) normalized errors of predicting individual seasonal AR models depending on month.

ical approach, Wiener–Granger causality estimation does not guarantee the uncovering of the cause-and-effect relation [34, 35], but is often much more effective than the approach based on the CCF analysis. The possibilities and features of the used method were considered, e.g., in [34–36].

The variance of the error of the process  $x_k$  predicted using an individual AR model divided by the variance  $x_k$  is denoted as  $\sigma_k^2$ , with index  $k$  characterizing the oceanic basin— $P$ ,  $A$ , and  $I$  for the PO, AO, and IO, respectively. In the analysis with special attention to IWP and IEP in the IO, we use for the index  $k$  the corresponding notations  $I_W$  and  $I_E$ . The order of AR models is determined using the Schwarz criterion [29, 30] and is denoted as  $d_k$ . The models used were only linear because the introduction of nonlinearity for the analyzed relatively short time series leads to a decrease in the statistical significance of the results and, complicating the analysis, often leaves the conclusions unchanged [29, 30]. For normalized improvements of the prediction, the following notation is introduced:

$G_{j \rightarrow k} = (\sigma_k^2 - \sigma_{k,j}^2) / \sigma_{k,j}^2$ , where  $j, k \in \{P, A, I\}$ ,  $j \neq k$ ,  $\sigma_{k,j}^2$  is the prediction error of the bivariate AR model of the process  $x_k$ ; the model contains  $d_{k,j}$  preceding values of the process  $x_j$  and the quantity  $d_{k,j}$  is deter-

mined by minimizing the estimate of the statistical significance level  $p(G_{j \rightarrow k})$  obtained by the  $F$ -test with the Bonferroni correction [29, 30, 37]. The less  $p(G_{j \rightarrow k})$ —the estimate of probability of a random error—the more reliable the conclusion about the presence of the impact  $j \rightarrow k$ . Values of  $G_{j \rightarrow k}$  characterize the intensity of the coupling  $j \rightarrow k$  [38] under conditions discussed in detail in [35, 36]. For clarity, they can be expressed in percentage. In the scope of linear AR models with allowance for the time of decorrelation of the analyzed processes (3–7 months), values of  $G_{j \rightarrow k}$  on the order of several percents are very significant for the observed variability and can correspond to a five- or sixfold larger unidirectional long-term effect—to an increase in the variance of the process  $x_k$  with the introduction of the coupling  $j \rightarrow k$  to the AR model when compared to the case of the absence of couplings [39]. The analysis involved the coefficient of proportionality between  $G_{j \rightarrow k}$  and long-term effect depending on the time of process decorrelation, as well as the correction for the nonlinearity of this dependence at sufficiently strong couplings [39].

If the third process  $x_i$  is taken into account, the coupling  $j \rightarrow k$  is characterized using the notation  $G_{j \rightarrow k|i} = (\sigma_{k,i}^2 - \sigma_{k,i,j}^2) / \sigma_{k,i}^2$ , where  $\sigma_{k,i,j}^2$  is the predic-

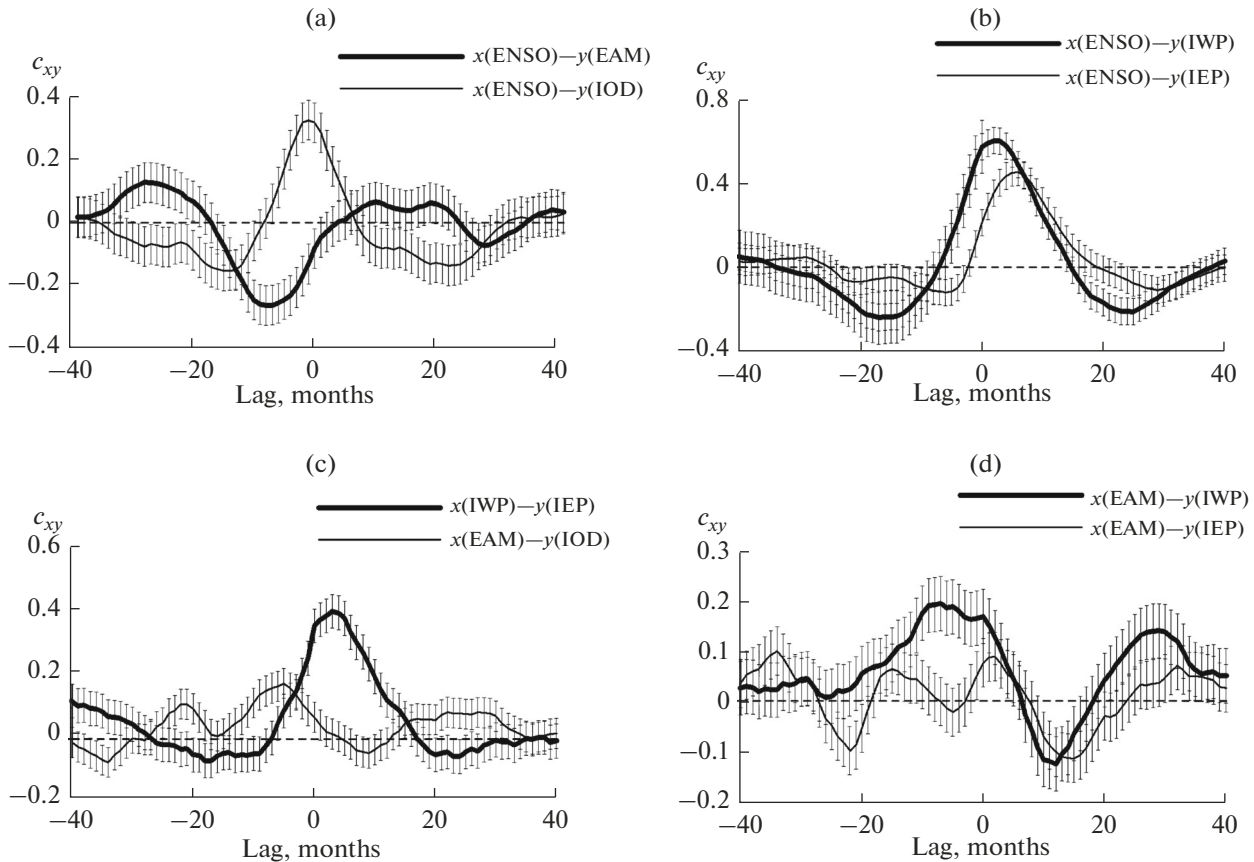


**Fig. 2.** Cross-correlation functions of the analyzed time series: (a) between ENSO and EAM, thick line; between ENSO and IOD, thin line; (b) between ENSO and IWP, thick line; between ENSO and IEP, thin line; (c) between IWP and IEP, thick line; between EAM and IOD, thin line; and (d) between EAM and IWP, thick line; between EAM and IEP, thin line. Vertical intervals are standard deviations of estimates by Bartlett's formula with allowance for autocorrelations.

tion error of the trivariate AR model containing  $d_{k,i,j}$  values of the process  $x_j$ . The value  $d_{k,i,j}$  is determined also by minimizing the significance level estimate  $p(G_{j \rightarrow k|i})$ . In the obtained AR model, the impact  $j \rightarrow k$  can be described not by one but by several (if  $d_{k,i,j} > 1$ ) coupling coefficients, which can have different signs. In this case, to characterize the "sign" of this coupling, it is suitable to highlight coupling coefficients that are maximum in the absolute value and presented below. When compared to bivariate analysis, taking into account the third process yields additional information. No conclusion about the presence of the direct impact  $j \rightarrow k$  can be made if the quantity  $G_{j \rightarrow k|i}$  is insignificant. At the same time,  $G_{j \rightarrow k|i}$  can be significant when  $G_{j \rightarrow k}$  is insignificant. This is implemented if the coupling  $j \rightarrow k$  occurs both directly and via the process  $x_i$ , even with different signs, and the total impact is weak; or, if  $x_j$  and  $x_i$  do not depend on each other and both have an effect on the process  $x_k$ . In

these two cases, the trivariate analysis is more sensitive for revealing the coupling when compared to the bivariate one.

In the analysis without taking into account the seasonal dependence, the corresponding coupling characteristics are hereinafter called nonseasonal. If the couplings significantly depend on the season and have different signs in different seasons, the nonseasonal (integral) estimate of  $G_{i \rightarrow k}$  can turn out to be almost zero and the coupling will not be revealed. For the processes considered in this work, the seasonal dependence of couplings and individual parameters can be strong due to the annual change in average climatologic characteristics, e.g., the ocean thermocline depth.

Coupling characteristics with allowance for the seasonal dependence with a period  $T$  (discrete time steps) were obtained using a modified method [40] in which the predicted values of the process  $x_k$  corresponded to the chosen season  $\tau$  and the analysis was carried out separately for each  $\tau$  from 1 to  $T$ . For the analysis of monthly average data,  $T = 12$  (from January to December); for the seasonal (three-month) data

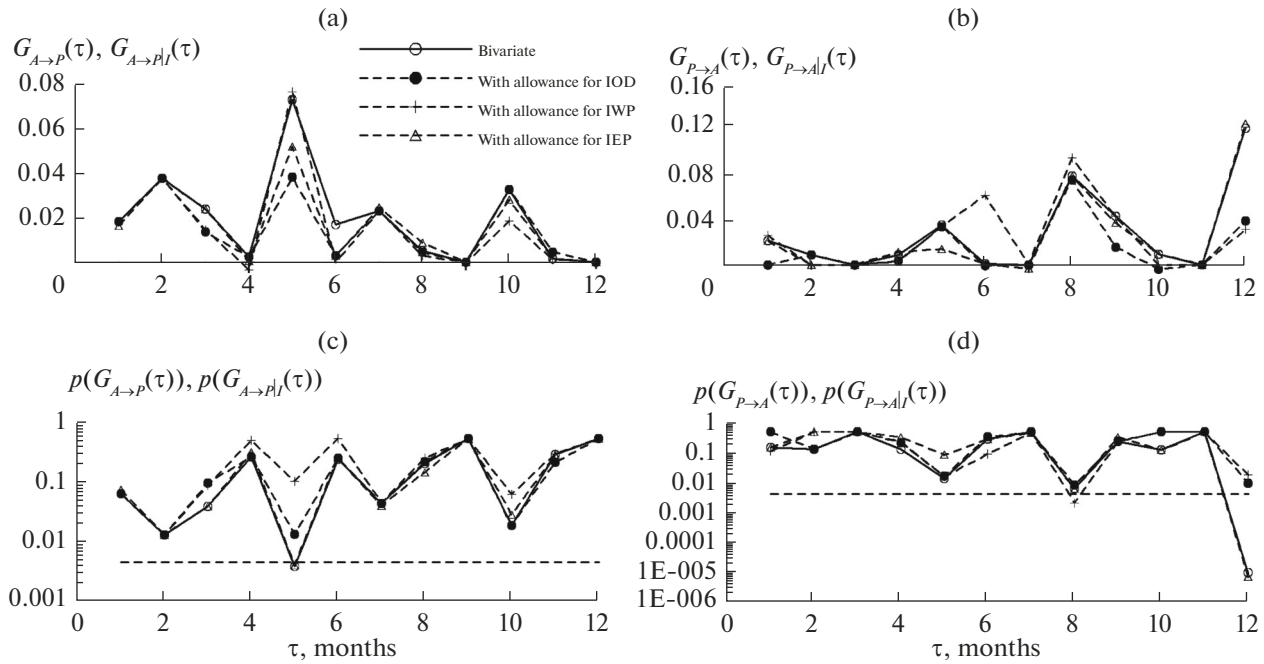


**Fig. 3.** Seasonal analysis of couplings between ENSO and EAM at month resolution: (a, b) characteristics of coupling (normalized improvements of the forecast) and (c, d) corresponding estimates for pointwise (for each individual month) significance. The horizontal dashed line is the level of 0.004 corresponding to the final significance level of 0.05. The left column (a, c) shows estimates of the EAM influence on ENSO; the right column (b, d) shows the influence of ENSO on EAM.

averaging,  $T = 4$  (in tropical latitudes, the seasons were defined as for the Northern Hemisphere: winter, from December to February; spring, from March to May; summer, from June to August; and autumn, from September to November); and, for data with semi-annual averaging (intervals from November to April and from May to October),  $T = 2$ . All characteristics were determined as functions of  $\tau$ :  $d_k(\tau)$ ,  $d_{k,j}(\tau)$ ,  $G_{j \rightarrow k}(\tau)$ ,  $p(G_{j \rightarrow k}(\tau))$ ,  $d_{k,i,j}(\tau)$ ,  $G_{j \rightarrow k|i}(\tau)$ , and  $p(G_{j \rightarrow k|i}(\tau))$  with allowance for an additional Bonferroni correction for trials of different  $\tau$ . The conclusion about nonzero  $G_{j \rightarrow k}(\tau)$  is made at the final significance level  $p$  if the pointwise significance level  $p(G_{j \rightarrow k}(\tau))$  is less than  $p/T$ .

Conclusions with the final significance level  $p \leq 0.05$  are usually considered sufficiently reliable. In the case of very small  $p \ll 10^{-4}$ , below it is stated only that  $p < 10^{-4}$  (a reliable conclusion).

### 4. RESULTS

The main results are presented for the most detailed—monthly—resolution. Together with this, the analysis was carried out for the 3- and 6-month resolution, because a rougher resolution can be useful if the couplings manifest themselves only on long time intervals. Its results are presented selectively.

To represent the accuracy of predictions of the obtained AR models, Fig. 1d presents seasonal dependences of prediction errors of individual AR models.

The prediction errors are minimum for the ENSO index and maximum for the IO indices.

#### 4.1. Estimates of the Mutual Influence of the AO and PO

The nonseasonal bivariate analysis by monthly data reveals a statistically significant influence of EAM on ENSO ( $G_{A \rightarrow P} = 2\%$ ) with a lag of  $d_{P,A} = 2$  months and negative coupling coefficient ( $-0.14$  with a delay of 2 months). According to [39], with allowance for the decorrelation times  $7\Delta t$  for  $x_P$  and  $3\Delta t$  for  $x_A$ , the long-term effect of the coupling  $A \rightarrow P$  (the unidirectional contribution of  $x_A$  to the variance of  $x_P$ ) was estimated as  $6G_{A \rightarrow P} \approx 12\%$ . Results of the trivariate analysis with allowance for  $x_I$  are similar. When using the IOD index as  $x_I$ , there are no differences between  $G_{A \rightarrow P}$  and  $G_{A \rightarrow P|I}$ . When using the IWP or IEP indices, the value was  $G_{A \rightarrow P|I} = 1.6\%$  with a unidirectional contribution of  $x_A$  to the variance of  $x_P$ ; the contribution was estimated as 10%. This slightly differs from results of the bivariate analysis.

With allowance for the seasonal dependence (Figs. 3a, 3c), the statistical significance of all estimates of the impact of EAM on ENSO is not so high, which is related to the reduction in data amount. In the bivariate analysis, a statistically significant impact of EAM on the May ENSO regime was revealed:  $G_{A \rightarrow P} = 7\%$ , final significance level  $p(G_{A \rightarrow P}) = 0.05$ , lag of 1 month, and

coupling coefficient  $-0.24$  with an error of  $0.22$ . With allowance for the IWP or IOD indices, the impact on the May ENSO regime also becomes insignificant (Figs. 3b, 3d); however, in the analysis of data with a 3-month resolution, a statistically significant estimate of the EAM impact on the spring ENSO regime was obtained even with allowance for the IWP or IOD indices.

Therefore, according to our results, the EAM impact on ENSO manifests itself with a lag of 2 months, negative coupling coefficient, and maximum in the spring season. The impact slightly depends on the IO state. It can cause up to 10% of variance of the index  $x_p$ .

The impact of ENSO on EAM in the nonseasonal bi- and trivariate analysis of data with a monthly (and rougher) resolution was not revealed. This testifies to the unidirectional coupling between EAM and ENSO, which was mentioned in [20, 22, 23].

In the seasonal bivariate analysis, the results are in general similar with a single exception. The dependence of December  $x_A$  the November index  $x_p$  is significant (Fig. 3c):  $G_{p \rightarrow A}(12) = 12\%$ , the final level  $p(G_{p \rightarrow A}) < 0.002$ , lag of 1 month, and coupling coefficient of  $0.09$  with an error of  $0.02$ . However, this dependence is insignificant with allowance for the IWP or IOD indices and, therefore, can be caused by the impact of the IO on ENSO and EAM.

#### 4.2. Estimates of the Mutual Influence of the AO and IO

The nonseasonal analysis of monthly data shows a statistically significant dependence of EAM on the IOD index ( $G_{I \rightarrow A} = 0.3\%$ ,  $p = 0.02$ ) and, somewhat weaker, on the IWP index ( $G_{I \rightarrow A} = 0.2\%$ ,  $p = 0.05$ ), although both the dependences are rather weak. At the same time, they manifest themselves noticeably more strongly in the analysis of data with 3-month resolution: the influence of IOD with  $G_{I \rightarrow A} = 1.7\%$ , positive coupling coefficient, and lag of 3 months is significant at a level  $p = 0.001$ ; the IWP influence is close in magnitude but has a longer lag (6 months) and is less significant ( $p = 0.007$ ). The mentioned characteristics of the lag testify that this coupling takes place on time scales larger than 1 month. Taking into account ENSO does not change these results. It should be noted that the dependence of the EAM index on IO indices (especially on IOD) was established reliably, in contrast to the dependence of EAM on ENSO.

The seasonal bivariate analysis yielded a significant estimate of the IWP influence on the December EAM regime:  $G_{I \rightarrow A}(12) = 10\%$ ,  $p(G_{I \rightarrow A}) < 0.0001$ , and lag of 1 month. The estimate of the IWP influence on the October EAM regime is significant and close in magnitude. The influence of IOD on EAM is somewhat less. In the seasonal trivariate analysis with allowance for ENSO, these influences become insignificant by analogy of how the influence of ENSO on EAM

becomes insignificant with allowance for the IWP or IOD regime. However, in the analysis of data with a 3-month resolution, dependences of the winter EAM regime on the IWP and IOD indices with allowance for ENSO become closer to significant ones (although only at level  $p = 0.1$ ); at semiannual resolution, the influence of IWP on the EAM regime in November–April is significant at a level of  $0.01$  also with allowance for the ENSO index.

It should be noted that the impact of the IO on EAM is revealed more stably at different time resolutions when compared to the impact of the PO on EAM. Together with the revealed significant impact of IOD (IWP) on EAM in the seasonal trivariate analysis, this testifies about the manifestation of the IOD (IWP) impact on EAM. As for the winter EAM regime, it strongly depends on the IO or ENSO indices or on both factors, which cannot be established more exactly by available data due to the correlation of the ENSO and IO indices.

As for the impact of EAM on processes in the IO, it does not manifest itself in the nonseasonal bivariate analysis. However, with allowance for ENSO, there appears the dependence of IWP on EAM ( $G_{A \rightarrow I|p} = 0.5\%$ ,  $p = 0.002$ ) and a somewhat weaker dependence of IEP on EAM ( $G_{A \rightarrow I|p} = 0.3\%$ ,  $p = 0.03$ ). The impacts of EAM on regions of IWP and IEP have the same positive sign and close coupling coefficients. The dependence of the IOD index on EAM is absent at any time resolution. According to these results, an increase in the EAM index leads to a weak—approximately similar in IWP and IEP—increase in the SST in the equatorial IO without an effect on the IOD index. The couplings are really weak—the presented improvement of the EAM prediction with allowance for the IWP index corresponds to the estimate of the long-term contribution of this coupling to the IWP variance of not more than 2%. In the seasonal analysis, the dependence of processes in the IO on EAM is insignificant.

#### 4.3. Estimates of the Mutual Influence of the PO and IO

The bivariate nonseasonal analysis by monthly data reveals a strong impact of ENSO on Indian Ocean processes, especially on the western pole of the dipole:

$G_{p \rightarrow I} \approx 8\%$ ,  $p < 10^{-4}$ , and lag of 1 month. The estimate of the unidirectional long-term contribution [39] of ENSO to the variance of the IWP index is 35%. The ENSO impact on the eastern pole of the dipole is somewhat weaker:  $G_{p \rightarrow I} \approx 5\%$ ,  $p < 10^{-4}$ , lag of 3 months; the long-term ENSO contribution to the variance of the IEP index is estimated as 25%. Both the impacts are with a positive coupling coefficient. The ENSO impact on the IOD index is weak,  $G_{p \rightarrow I} < 1\%$ , and the significance is not high,  $p = 0.04$ .

The seasonal analysis reveals a significant ENSO influence on Indian Ocean processes characterized by the three indices used. In general, the strongest impact was revealed on the IWP region. It is statistically significant in all months but July. It is maximum in October ( $G_{p \rightarrow I}(10) = 23\%$ ,  $p < 10^{-4}$ , lag of 1 month, and the coupling coefficient of 0.12 with an error of 0.02). In winter months, the ENSO impact on the IWP region is weaker. At the same time, a strong ENSO impact on the IEP region appears; this impact is significant from November to April, but is maximum in winter. The maximum value is reached in January ( $G_{I \rightarrow 3}(1) = 25\%$ ,  $p < 10^{-4}$ , lag of 1 month, and the coupling coefficient of 0.13 with an error of 0.02).

The ENSO influence on the IOD index is weaker; it manifests itself from August to October, with a maximum in October ( $G_{p \rightarrow I}(10) = 11\%$ ,  $p = 0.0003$ , lag of 1 month, and a coupling coefficient of 0.13 with an error of 0.03). The latter manifests itself due to the ENSO impact on the IWP region, not on the IEP region. A rougher time resolution yields the same results, which verifies the continuous ENSO impact on IWP with the maximum influence on the autumn IWP regime, as well as the ENSO impact on the winter IEP regime and on the autumn IOD regime. In the trivariate analysis with allowance for EAM, the estimates are almost the same. In general, a strong ENSO impact on the SST regime takes place in the Indian Ocean. In addition to the nonseasonal analysis, which revealed a stronger impact on the IWP region, seasonal estimates testify that the ENSO impact from spring to summer is considerably stronger on the IWP region; in winter it is stronger on the IEP region.

The impact of Indian Ocean processes on ENSO manifests itself in the nonseasonal bivariate analysis by monthly data. The IEP influence is the strongest:

$G_{I \rightarrow p} \approx 4\%$ ,  $p < 10^{-4}$ , lag of 5 months, with a negative sign. The unidirectional contribution of SST variations in the IEP region to the variance of the ENSO index is estimated as 20%. The dependence of ENSO on the IOD index manifests itself more weakly:  $G_{I \rightarrow p} \approx 2\%$ ,  $p < 10^{-4}$ , and a lag of 6 months. The impact of IWP is weaker:  $G_{I \rightarrow p} \approx 1\%$ ,  $p = 0.001$ . The nonseasonal trivariate analysis with allowance for EAM yields close results, with some decrease in estimates of the impact force.

The seasonal analysis revealed the strongest impact of Indian Ocean processes on ENSO when using the IEP index: this is the influence on the August ENSO regime ( $G_{I \rightarrow p} = 9\%$ ,  $p = 0.01$ , and lag of 2 months; the coupling coefficient with a lag of 2 months is  $-0.4$  with an estimate of the error of 0.13) and on the June regime ( $G_{I \rightarrow p} = 5\%$ ,  $p = 0.05$ , lag of 1 month, and coupling coefficient of  $-0.32$  with an estimate of the error of 0.11). This impact also manifests itself with allowance for EAM. The IWP impact on the May and

June ENSO regimes is somewhat less significant and has a longer lag; however, it becomes insignificant with allowance for EAM. The seasonal analysis did not reveal the dependence of ENSO on the IOD index.

#### 4.4. Analysis of Couplings with the Simultaneous Taking into Account the IWP and IEP Indices

To characterize the part of each of the IOD poles, as well as of the IOD and average SST for IEP and IWP (we denote it as IOD(a)), the triples ENSO–IEP–IWP, ENSO–IOD–IOD(a), EAM–IEP–IWP, and EAM–IOD–IOD(a) were analyzed.

Nonseasonal analysis verifies that the dependence of ENSO on IWP and other IO indices does not manifest itself if IEP is taken into account. The results testify that the IO has an effect on ENSO only via the eastern pole. This is also corroborated by the seasonal analysis with a monthly resolution. The IWP impact on ENSO manifests itself only at 3-month and semi-annual resolution (mostly on the summer regime).

As for couplings within the IO, the estimates testify about the IEP impact on IWP with the negative sign and IWP impact on IEP with the positive sign. The impact of IOD on IOD(a) with the positive sign and that of IOD(a) on IOD with the negative sign also take place. These interregional interactions within the IO are not very strong—they are weaker than the interaction of individual IO regions with ENSO. They are stronger than couplings of the IO and EAM. Taking them into account in general has no effect on the conclusions made above about the mentioned different part of the IWP, IEP and IOD indices as indicators of processes in regions of the equatorial Indian Ocean in the analysis of couplings with processes in equatorial Pacific and Atlantic oceans.

#### 4.5. General Scheme of Key Couplings

Figures 4a and 4b present a scheme characterizing the main, most significant, and stable couplings revealed in this work. The arrows show directions of couplings, and line thickness qualitatively characterizes the relative force of the couplings. Table 1 shows values  $G_{j \rightarrow k|i}$  for a one-month-ahead forecast, significance level  $p(G_{j \rightarrow k|i})$ , maximum in absolute value coupling coefficient in the AR model ( $a_{\max}$ ), lag of coupling (number of coupling coefficients  $d_{k,i,j}$  multiplied by  $\Delta t = 1$  month), and the season of the maximum manifestation.

The strongest couplings were revealed between ENSO and Indian Ocean processes. El Niño phenomena lead to an increase in temperature both in the IWP region and in the IEP region (Fig. 4b). In this process, the SST first increases in the IWP region (lag of 1 month; the influence manifests itself maximally in the autumn season, although is also

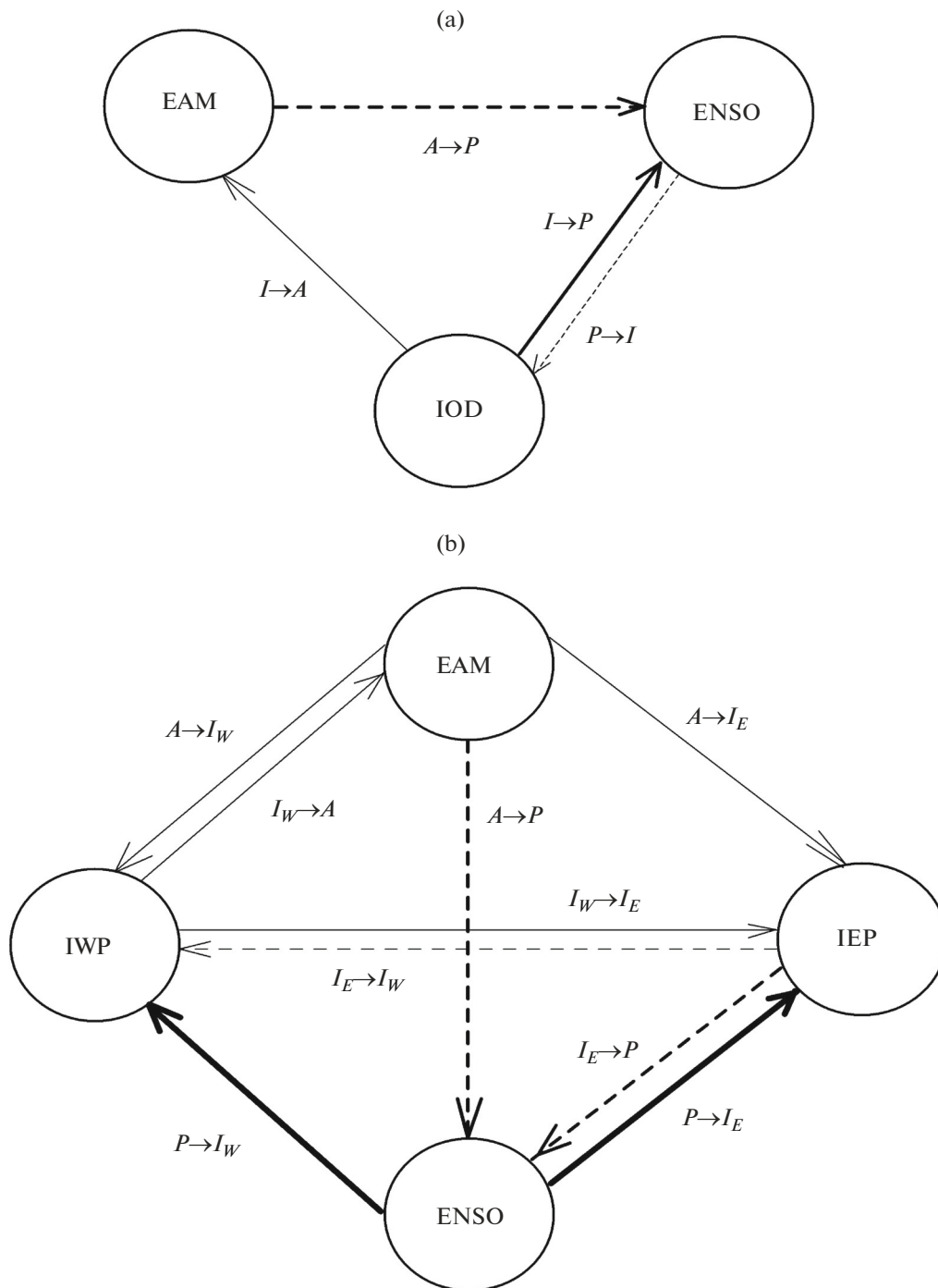


**Fig. 4.** Schemes of the revealed couplings between OST variations of tropical oceans: (*P*) Pacific, (*A*) Atlantic, and (*I*) Indian: when using (a) IOD or (b) IWP and IEP for the characterization of processes in the Indian Ocean. Solid lines characterize impacts with positive coupling coefficients, dashed lines show impacts with negative coefficients, and the dotted line ( $P \rightarrow I$ ) shows impacts with coupling coefficients with different signs—their sum is close to zero. Thick lines characterize the most significant couplings: (a) EAM and IOD on ENSO and (b) ENSO on IWP and IEP (and, somewhat weaker, EAM and IEP on ENSO). Quantitative characteristics of the relations are presented in Table 1.

large in other seasons). Then, the OST increases in the IEP region (the lag of the coupling is 3 months; the influence manifests itself maximally in the winter season). The SST in the IEP region increases both under the direct impact of ENSO and under the

impact of IWP. The influence of ENSO on the IOD index is much weaker (Fig. 4a). This points to the fact that El Niño favors the relatively homogeneous increase in the SST in the equatorial IO, not the change in the SST zonal gradient. In turn, the

**Table 1.** Characteristics of main revealed relations

	$G_{i \rightarrow j k}$ , %	$p(G_{i \rightarrow j k})$	$a_{\max}$	Lag, months	Season of the maximum
$A \rightarrow P$	<b>1.6</b>	<b>&lt;0.0001</b>	<b><math>-0.13 \pm 0.06</math></b>	<b>2</b>	<b>Spring NH</b>
$I \rightarrow P$	<b>1.8</b>	<b>&lt;0.0001</b>	<b><math>0.14 \pm 0.05</math></b>	<b>1</b>	—
$I_W \rightarrow P$	0.6	0.02	$-0.11 \pm 0.10$	3	—
$I_E \rightarrow P$	<b>3.6</b>	<b>&lt;0.0001</b>	<b><math>-0.12 \pm 0.08</math></b>	<b>5</b>	<b>Summer NH</b>
$P \rightarrow I$	0.7	0.04	No clear maximum among six coupling coefficients	6	Autumn NH
$P \rightarrow I_W$	<b>7.5</b>	<b>&lt;0.0001</b>	<b><math>0.07 \pm 0.01</math></b>	<b>1</b>	<b>Autumn NH</b>
$P \rightarrow I_E$	<b>5.3</b>	<b>&lt;0.0001</b>	<b><math>0.04 \pm 0.03</math></b>	<b>3</b>	<b>Winter NH</b>
$I \rightarrow A$	0.4	0.01	$0.05 \pm 0.04$	1	Winter NH
$I_W \rightarrow A$	0.2	0.05	$0.04 \pm 0.04$	1	Winter NH
$A \rightarrow I_W$	0.5	0.002	$0.03 \pm 0.02$	1	—
$A \rightarrow I_E$	0.3	0.03	$0.02 \pm 0.02$	1	—

Improvement of a one-month-ahead forecast in nonseasonal trivariate analysis  $G_{i \rightarrow j|k}$ , significance level  $p(G_{i \rightarrow j|k})$ , maximum in the absolute value coupling coefficient in the AR model  $a_{\max}$  with a 95% confidence interval, lag of the coupling, and season of the maximum manifestation of the coupling (lines indicates the absence of a clear maximum in the seasonal analysis). The most significant couplings are highlighted (corresponding to the thick arrows in Fig. 4).

increase in temperature in the IEP region has a strong effect on the SST in the region of the El Niño formation (in the region of Niño 3.4, the effect is maximum for the summer season) with a negative coupling coefficient. This must favor the formation of a La Niña type regime with negative anomalies of the SST in equatorial PO regions. The impact of the IO on ENSO is implemented via SST variations in the IEP region (Fig. 4b). According to the obtained estimates of (unidirectional) long-term effects [39], the ENSO influence can cause up to 35% of the variance for the IWP index and 25% of the variance for the IEP index. The influence of SST variations in the IEP region, in turn, can cause up to 20% of the variance of the ENSO index.

The interaction between EAM and the mentioned processes manifests itself much more weakly. Only the impact of EAM on the ENSO regime (maximally, in spring) manifests itself noticeably with a lag of 2 months and negative coupling coefficient; i.e., the increase in the SST in the eastern equatorial Atlantic favors manifestations typical for the La Niña phenomena in the PO. The (unidirectional) EAM contribution to the variance of the ENSO index is estimated as about 10%. The EAM impact on IWP and IEP is much weaker (Fig. 4b): less than 1% of the improvement of the monthly forecast and unidirectional contribution to the variance of no more than 2–3%, without clear maximums in the annual cycle, and positive coupling coefficients (an increase in the SST in Atlantic causes a weak growth of the SST both in IWP and in IEP).

Nonseasonal analysis reveals the impact of IOD (Fig. 4a) and, just weaker, of IWP (Fig. 4b) on EAM.

This is influence with a positive coupling coefficient; its unidirectional contribution to the EAM variance is no more than 2–3%. As for the influence of ENSO on EAM, it does not manifest itself in nonseasonal analysis.

A dependence of the winter EAM regime on ENSO or on IOD (or IWP) was revealed. The high correlation between winter indices of ENSO and IWP complicates revealing a preferable interaction process from the available data. The average impact of IOD (IWP) and ENSO on EAM for all seasons manifests itself weakly in all cases (Figs. 4a, 4b).

## 5. CONCLUSIONS

The new results corroborate only some of the hypotheses, mechanisms, and coupling estimates proposed earlier. Our results significantly specialize estimates of couplings in tropical latitudes of three oceans with allowance for the seasonal dependence. The presence of the EAM impact on ENSO with a negative coupling coefficient is corroborated as in [20, 22, 23]. Seasonal analysis reveals that this impact is maximum in the spring season of the Northern Hemisphere. No impact of ENSO on EAM was revealed on average for all seasons, in contrast to [12, 14], and the impact of IO on EAM takes place, although relatively weakly. We noted that, in the winter season, the dependence of EAM on IOD (IWP) or on ENSO, or on both processes, appears. The results testify only about rather weak EAM impacts on Indian Ocean processes.

The ENSO impact on Indian Ocean processes, which was frequently mentioned earlier, has been cor-

roborated. In connection with this, a stronger ENSO impact on IWP, as well as the impact of the IEP and IOD regimes on ENSO, have been revealed. The impact of ENSO on IOD is estimated as weak and is not highlighted among main results (in contrast to [22, 24]). It is natural to relate the somewhat larger part of this impact in [22, 24] to the difference in methods of analysis and smaller amount of the analyzed data. In this work, the analysis involved AR models with optimally tuned dimensions (not the a priori given dimension 1 or 2) and the analyzed time interval is three times as long as in [22]. Along with it, in this work the significance of conclusions is estimated; in [24], only point estimates were presented. According to the results for the seasonal dependence, the ENSO impact on the autumn (for the Northern Hemisphere) IWP regime and, then, on the winter IEP regime is strongest. The inverse impact of Indian Ocean processes is implemented via SST variations in the IEP region with a maximum in summer.

Thus, the seasonal trivariate analysis resulted in additional characteristics of couplings between ENSO, EAM, and IOD (IWP, IEP) when compared to previous works. Among the results, seasonal characteristics of the EAM impact on ENSO, the ENSO impact on the IWP and IEP regime, the impact of the IEP regime on ENSO, and the impacts of IWP and IOD regimes on EAM can be treated as the main ones.

#### ACKNOWLEDGMENTS

This work was supported by the Government of the Russian Federation (agreement no. 14.Z50.31.0033 with the Institute of Applied Physics of RAS), the Russian Academy of Sciences, and the Russian Foundation for Basic Research (project nos. 14-05-00639 and 14-02-00492). Eddy-wave features of the process under study were analyzed in the scope of project no. 14-17-00806 of the Russian Science Foundation.

#### REFERENCES

1. *Climate Change 2013: The Physical Science Basis. Contribution of Working Group I to the Fifth Assessment Report of the Intergovernmental Panel on Climate Change*, Ed. by T. F. Stocker, D. Qin, G.-K. Plattner, (Cambridge Univ. Press, Cambridge, 2013).
2. P. Chang, T. Y. Yamagata, P. Schopf, et al., "Climate fluctuations of tropical coupled systems—the role of ocean dynamics," *J. Clim.* **19**, 5122–5174 (2006).
3. K. Arpe, L. Bengtsson, G. S. Golitsyn, et al., "Analysis and modeling of the hydrological regime variations in the Caspian Sea basin," *Dokl. Earth Sci.* **366** (4), 552–556 (1999).
4. V. I. Byshev, *Synoptic Large-Scale Variability of the Ocean and Atmosphere* (Nauka, Moscow, 2003) [in Russian].
5. I. I. Mokhov and V. Ch. Khon, "Interannual variability and long-term tendencies of change in atmospheric centers of action in the Northern Hemisphere: Analyses of observational data," *Izv., Atmos. Ocean. Phys.* **41** (6), 657–666 (2005).
6. I. I. Mokhov, "Specific features of the 2010 summer heat formation in the European territory of Russia in the context of general climate changes and climate anomalies," *Izv., Atmos. Ocean. Phys.* **47** (6), 653–660 (2011).
7. I. I. Mokhov, E. M. Dobryshman, and M. E. Makarova, "Transformation of tropical cyclones into extratropical: The tendencies of 1970–2012," *Dokl. Earth Sci.* **454** (1), 59–63 (2014).
8. I. I. Mokhov and A. V. Timazhev, "Assessment of the predictability of climate anomalies in connection with El Niño phenomena," *Dokl. Earth Sci.* **464** (2), 1089–1093 (2015).
9. J. Merle, "Variabilité thermique annuelle et interannuelle de l'océan Atlantique équatorial Est. L'hypothèse d'un el "El Niño" Atlantique," *Oceanol. Acta* **3** (2), 209–220 (1980).
10. S. E. Zebiak, "Air–sea interaction in the equatorial Atlantic region," *J. Clim.* **6**, 1567–1586 (1993).
11. N. H. Saji, B. N. Goswami, P. N. Vinayachandran, and T. Yamagata, "A dipole mode in the tropical Indian Ocean," *Nature* **401**, 360–363 (1999).
12. M. Latif and T. P. Barnett, "Interaction of the tropical oceans," *J. Clim.* **8**, 952–964 (1995).
13. D. B. Enfield and D. A. Mayer, "Tropical Atlantic sea surface temperature variability and its relation to El Niño–Southern Oscillation," *J. Geophys. Res.* **102**, 929–945 (1997).
14. M. Latif and A. Groetzner, "The equatorial Atlantic oscillation and its response to ENSO," *Clim. Dyn.* **16**, 213–218 (2000).
15. A. Ruiz-Barradas, J. A. Carton, and S. Nigam, "Role of the atmosphere in climate variability of the tropical Atlantic," *J. Clim.* **16**, 2052–2065 (2003).
16. S.-P. Xie and J. A. Carton, "Tropical Atlantic variability: Patterns, mechanisms, and impacts," in *Earth Climate: The Ocean–Atmosphere Interaction*, Ed. by C. Wang, S.-P. Xie, and J. A. Carton (AGU, Washington D.C., 2004), pp. 121–142.
17. C. Wang, "ENSO, Atlantic climate change variability, and the Walker and Hadley circulations," in *The Hadley Circulation: Present, Past and Future*, Ed. by H. F. Diaz and R. S. Bradley (Kluwer, Dordrecht, 2005), pp. 173–202.
18. C. Deser, A. Capotondi, R. Saravanan, and A. S. Phillips, "Tropical Pacific and Atlantic climate variability in CCSM3," *J. Clim.* **19**, 2451–2481 (2006).
19. P. Chang, Y. Fang, R. Saravanan, L. Ji, and H. Seidel, "The cause of the fragile relationship between the Pacific El Niño and the Atlantic Niño," *Nature* **443**, 324–328 (2006).
20. S. S. Kozlenko, I. I. Mokhov, and D. A. Smirnov, "Analysis of the cause and effect relationships between El Niño in the Pacific and its analog in the equatorial Atlantic," *Izv., Atmos. Ocean. Phys.* **45** (6), 704–713 (2009).
21. C. Wang, F. Kucharski, R. Barimalala, and A. Bracco, "Teleconnections of the tropical Atlantic to the tropical Indian and Pacific oceans: A review of recent findings," *Meteorol. Z.* **18** (4), 445–454 (2009).

22. M. F. Jansen, D. Dommenges, and N. Keenlyside, "Tropical atmosphere–ocean interactions in a conceptual framework," *J. Clim.* **22**, 550–567 (2009).
23. H. Ding, N. Keenlyside, and M. Latif, "Impact of the equatorial Atlantic on the El Niño Southern Oscillation," *Clim. Dyn.* **38**, 1965–1972 (2012).
24. X. San Liang, "Unraveling the cause–effect relation between time series," *Phys. Rev. E* **90**, 052150 (2014).
25. J. Bjerknes, "A possible response of the atmospheric Hadley circulation to equatorial anomalies of ocean temperature," *Tellus* **18**, 820–829 (1966).
26. J. Bjerknes, "Atmospheric teleconnections from the equatorial Pacific," *J. Phys. Oceanogr.* **97** (3), 163–172 (1969).
27. I. I. Mokhov and D. A. Smirnov, "El Niño Southern Oscillation drives North Atlantic Oscillation as revealed with nonlinear techniques from climatic indices," *Geophys. Res. Lett.* **33**, L03708 (2006). doi 10.1029/2005GL024557
28. I. I. Mokhov and D. A. Smirnov, "Study of the mutual influence of the El Niño–Southern Oscillation processes and the North Atlantic and Arctic oscillations," *42* (5), 598–614 (2006).
29. I. I. Mokhov, D. A. Smirnov, P. I. Nakonechny, et al., "Alternating mutual influence of El-Niño/Southern Oscillation and Indian monsoon," *Geophys. Res. Lett.* **38**, L00F04 (2011). doi 10.1029/2010GL045932
30. I. I. Mokhov, D. A. Smirnov, P. I. Nakonechny, S. S. Kozlenko, and J. Kurths, "Relationship between El-Niño/Southern Oscillation and the Indian monsoon," *Izv., Atmos. Ocean. Phys.* **48** (1), 47–56 (2012).
31. J. Runge, J. Kurths, and V. Petoukhov, "Quantifying the strength and delay of climatic interactions: The ambiguities of cross correlation and a novel measure based on graphical models," *J. Clim.* **27**, 720–739 (2014).
32. N. Wiener, "Theory of prediction," in *Modern Mathematics for the Engineer*, Ed. by E. F. Beckenbach (McGraw-Hill, New York, 1956), pp. 166–186.
33. C. W. J. Granger, "Investigating causal relations by econometric models and cross-spectral methods," *Econometrica* **37** (3), 424–438 (1969).
34. D. A. Smirnov and B. P. Bezruchko, "Spurious causalities due to low temporal resolution: Towards detection of bidirectional coupling from time series," *Europhys. Lett.* **100**, 10005 (2012).
35. D. A. Smirnov, "Spurious causalities with transfer entropy," *Phys. Rev. E* **87**, 042917 (2013).
36. D. A. Smirnov and I. I. Mokhov, "Estimation of interaction between climatic processes: Effect of sparse sample of analyzed data series," *Izv., Atmos. Ocean. Phys.* **49** (5), 485–493 (2013).
37. E. Lehmann, *Testing Statistical Hypotheses* (Wiley, New York, 1959; Nauka, Moscow, 1979).
38. D. A. Smirnov, "Quantifying causal couplings via dynamical effects: A unifying perspective," *Phys. Rev. E* **90**, 062921 (2014).
39. D. A. Smirnov and I. I. Mokhov, "Relating Granger causality to long-term causal effects," *Phys. Rev. E* **92**, 042138 (2015).
40. I. I. Mokhov and D. A. Smirnov, "The trivariate seasonal analysis of couplings between El Niño, North Atlantic Oscillation, and Indian monsoon," *Russ. Meteorol. Hydrol.* **41** (11–12), 798–807 (2016).

*Translated by A. Nikol'skii*